The Interplay between Viscoelastic and Thermodynamic Properties Determines the Birefringence of F-Actin Gels

Emmanuèle Helfer,* Pierre Panine,† Marie-France Carlier,* and Patrick Davidson‡

*Dynamique du Cytosquelette, Laboratoire d'Enzymologie et Biochimie Structurales, UPR 9063 Centre National de la Recherche Scientifique, Gif-sur-Yvette, France; †European Synchrotron Radiation Facility, Grenoble, France; and ‡Laboratoire de Physique des Solides, UMR 8502 Centre National de la Recherche Scientifique, Université Paris-Sud, Orsay, France

ABSTRACT F-actin gels of increasing concentrations (25–300 μM) display in vitro a progressive onset of birefringence due to orientational ordering of actin filaments. At F-actin concentrations $<$100 μM, this birefringence can be erased and restored at will by sonication and gentle flow, respectively. Hence, the orientational ordering does not result from a thermodynamic transition to a nematic phase but instead is due to mechanical stresses stored in the gels. In contrast, at F-actin concentrations $\geq$100 μM, gels display spontaneous birefringence recovery, at rest, which is the sign of true nematic ordering, in good agreement with statistical physics models of the isotropic/nematic transition. Well-aligned samples of F-actin gels could be produced and their small-angle x-ray scattering patterns are quite anisotropic. These patterns show no sign of filament positional short-range order and could be modeled by averaging the form factor with the Maier-Saupe nematic distribution function. The derived nematic order parameter S of the gels ranged from $S = 0.7$ at 300 μM to $S = 0.4$ at 25 μM. Both birefringence and small-angle x-ray scattering data indicate that, even in absence of cross-linking proteins, spontaneous cooperative alignment of actin filaments may arise in motile regions of living cells where F-actin concentrations can reach values of a few 100 μM.

INTRODUCTION

A major function of cytoskeletal filaments is to support cell structure, either for mechanical stability (e.g., resistance to external forces, adhesion, reinforcement) or for motile processes (e.g., cell division, mitosis, migration). The most abundant of these cytoskeletal proteins is actin. Monomeric actin, or G-actin, polymerizes in the presence of K^+ or Mg^{2+} to form helical polar filaments, or F-actin, of a few tens of micrometers long and ~7–8 nm in diameter; F-actin is involved in many motile phenomena (e.g., protrusion, endocytosis) which are conventionally called actin-based motility processes. Actin and its regulators are well-characterized biochemically (see Pollard et al. (1) for review). The concepts of polymerization/depolymerization and critical monomer concentration of actin have been developed by Oosawa (2). However, the irreversible hydrolysis of the bound ATP nucleotide associated with actin polymerization destabilizes the filament and is at the origin of an important feature called treadmilling (3). In the absence of ATP, polymerization is reversible and an equilibrium between G-actin and F-actin is reached at a critical concentration c_c of G-actin, identical at the two ends. In the presence of ATP, the polymerization is no longer reversible, which induces a difference of c_c between the two filament ends: one end (the barbed end) polymerizes whereas the other one (the pointed end) depolymerizes at the same rate, resulting in a filament of apparent constant length with a continuous flux of subunits through it. By continuously renewing the actin filament, which is, therefore, moving and able to generate forces, this treadmilling process is the basis of cellular motility. Many of the cellular structures observed in these dynamic processes display aligned organizations of parallel actin filaments. Actin-binding proteins (ABPs) are involved in these motile processes observed in vivo. They interact specifically with F-actin to form three-dimensional complex structures of various types like the dense branched array in the lamellipodium or the tight filaments bundles in microvilli. Interestingly, it has been observed in vitro that actin filaments can form aligned structures in the absence of regulating ABPs at physiological conditions. Basic physical mechanisms underlying spontaneous F-actin alignment are important to understand dynamic changes in cytoplasmic structures occurring during cell movements. For these reasons, F-actin-based structures have recently attracted much interest from the structural and physical points of view.

Many biomimetic studies have been realized in which actin filaments were associated with cross-linking proteins or membranes to mimic structures observed in vivo in cells. Actin filaments were either cross-linked by α-actinin or by filamin to form networks and fibers that displayed a variety of biologically relevant mechanical properties (4,5). Alternatively, the interaction of F-actin with phospholipid membranes modified the dynamics of the membrane, mimicking the cortical network (4,6–9).

To understand the mechanical properties of such complex structures, one needs first to define the microscopic properties of individual filaments as a starting point for modeling, in a later stage, the macroscopic properties of F-actin

Submitted July 23, 2004, and accepted for publication April 26, 2005.

Address reprint requests to Emmanuèle Helfer, LEBS, UPR 9063 CNRS, 1 Avenue de la Terrasse, F-91198, Gif-sur-Yvette, France. Tel.: 33-0-1-698-23480; Fax: 33-0-1-698-23129; E-mail: helfer@lebs.cnrs-gif.fr.

0006-3495/05/07/543/11 $2.00

doi: 10.1529/biophysj.104.050245

architectures. By comparison with synthetic flexible polymers, these biopolymers are characterized by a large persistence length L_p of ~5–20 μm (10–12), ~3 orders-of-magnitude larger than their diameter D (L_p is on the order of a nanometer for flexible polymers). They are thus called semiflexible polymers. Due to their large aspect ratio L_p/D, actin filaments form semidilute solutions at extremely low volume fractions and display unique network (i.e., gels) properties such as, e.g., an elastic modulus much larger than that of flexible polymers at the same volume fraction. Because of their length and extended configuration, actin filaments cannot diffuse in solution without steric interaction with neighboring filaments. As a result, F-actin solutions become highly viscous at low concentrations and can form viscoelastic solids at molarities similar to those found in the cytoplasm. Because this viscoelastic character is important for the role of actin networks in the cell cytoskeleton, actin viscoelastic properties have been extensively studied theoretically (13–15) and experimentally (16–18) in the past years. Theoretical models combining the individual mechanical properties of actin filaments with those of membranes were established to explain the results observed with actin-coated membranes (19).

In comparison with rheological and theoretical studies on viscoelasticity of actin gels, the properties of orientational ordering of actin have been less studied, both theoretically and experimentally. Actin gels have raised interest because they exhibit birefringence that is due to the parallel alignment of actin filaments. Such birefringence is usually regarded as the sign of a liquid-crystalline nematic order. However, for all other nematic liquid crystals, a clearcut first-order transition is observed between the nematic phase at high concentration and the isotropic phase at low concentration (20). This means that the two phases should coexist in a given concentration range. The phase separation shows up at the microscopic scale by the appearance of small nematic droplets within the isotropic phase. At the macroscopic scale, samples held in test-tubes spontaneously demix under the influence of gravity into a top isotropic phase and a bottom birefringent nematic phase (21). Actin gels behave differently. They show a gradual onset of birefringence as concentration increases rather than the expected phase coexistence. So far a single report has provided indirect evidence, at the microscopic scale, for nematic and isotropic domains in actin gels (22). In another report, actin gels were thought to represent a unique example of a continuous isotropic to nematic phase transition (23). Such a continuous second-order transition, instead of a first-order one, is theoretically possible and was predicted by Toner's group (24–26). In addition to showing a gradual onset of birefringence, the nematic ordering is predicted to be very weak and topological defects of the nematic order, called disclination lines, are not expected to occur. One basic assumption of the theory is that the system reaches thermodynamic equilibrium, which may not actually be fulfilled in the case of actin gels. In addition to birefringence, actin gels indeed display strong viscoelastic properties that may severely affect their phase behavior as mentioned above. We think that a combination of the viscoelastic and liquid crystalline properties of actin may shed light on the functional and structural properties of the complex actin structures that are assembled in vivo.

In this context, we decided to reexamine the thermodynamic and structural properties of pure F-actin suspensions: this work will provide a reference state to discuss more complicated structures such as actin fibers and actin networks that can be observed in cells, and that are regulated by ABPs. On this basis, the effect of the addition of regulating proteins could be investigated in the future in order to be closer to in vivo conditions. In this study, we consider two sides of this question: Firstly, we investigate the nature of the isotropic to nematic phase transition (*I-N* transition) in actin gels prepared in test tubes. Secondly, we report anisotropic x-ray scattering patterns of gels of actin filaments aligned by flow in capillaries, which helps us to understand the molecular organization of these materials. Since the local concentration of actin in filament arrays that are assembled in actin-based motile processes like lamellipodia or actin tails of rocketing particles can be as high as 0.2–1 mM (27,28), we decided to investigate a broad range of actin concentrations to obtain physiologically relevant information. We show that the observed macroscopic birefringence is of thermodynamic origin above a threshold of 100 μM, whereas it is due only to mechanical stress below this threshold. However, the second kind of experiment (i.e., small-angle x-ray scattering) indicates that the actin gels, sheared in capillaries in order to align the filaments, present a large order parameter indicating a strong filaments orientation, even at concentrations as low as 25 μM.

MATERIALS AND METHODS

Actin purification and concentration

Actin was purified from rabbit muscle according to the method described by Spudich and Watt (29). Actin was finally isolated in the monomeric Ca-ATP-G form by gel filtration on Superdex 200 (Amersham, Little Chalfont, Buckinghamshire, UK) in G buffer (5 mM Tris, pH 7.8, 1 mM DTT, 0.1 mM $CaCl_2$, 0.2 mM ATP, 0.01% NaN_3). Fractions representing 50% of the material in the second half of the actin peak were collected, to avoid any contamination of actin dimers. Actin purity was assessed by the presence of a single band on SDS-PAGE, and α-actinin (the major potential actin-bundling factor in muscle actin) was not detectable by immunodetection. ATP-G-actin (generally at 50 $\pm$ 10 μM) was stored at 0°C (on ice) in G buffer.

G-actin was concentrated by ultrafiltration using a Vivaspin 30 device (Vivascience, Göttingen, Germany) centrifuged at 5000 *g* for a few hours, at 4°C, to reach a concentration of ~300 μM. The final concentration was measured either by the bicinchoninic acid assay or by measuring the solution absorption at 290 nm. Due to their very high viscosities the concentrated G-actin solutions showed inhomogeneities visible in the spectrophotometer cuvettes. The actin concentration could therefore be measured with a 20% accuracy, depending on the sample region probed.

Actin polymerization

Ca-G-actin was polymerized into Mg-F-actin by adding 100 mM KCl, 1 mM $MgCl_2$, and 0.2 mM EGTA (F buffer). Polymerization occurred in a few minutes on ice. The solution of Mg-F-actin could be kept at room temperature for the day.

Test tubes: visual inspection in polarized light

Concentrated G-actin was diluted with G buffer to desired concentrations (25–250 μM) in glass test tubes (~9 mm in diameter) to a final volume of 500 μl. Actin was polymerized directly in the test tube by adding 25 μl of KME solution (2 M KCl, 20 mM $MgCl_2$, 4 mM EGTA). The series of test tubes was observed in polarized light (the tubes were held between two crossed polarizers and illuminated in white light).

Sonication

An ultrasonic probe (VibraCell, Sonics & Materials, Danbury, CT) was inserted into the test tube to sonicate the F-actin gels and disrupt birefringent structures. Sonication was applied continuously for 10–30 s, then the ultrasonic probe was slowly removed from the solution to avoid any flow that could induce artifactual flow birefringence. Resulting changes in the birefringence were observed in polarized light.

Capillaries: polarized-light microscopy and x-ray scattering

For polarized-light microscopy, samples were prepared by inserting F-actin solutions into flat glass capillary tubes (VitroCom, Mountain Lakes, NJ) of thicknesses ranging from 50 to 200 μm. This was achieved either by capillary rise in the case of fluid enough F-actin solutions or by gently sucking F-actin gels with help of a syringe or a small vacuum pump. The capillaries were flame-sealed at each end, taking care not to heat the sample.

For x-ray scattering measurements, F-actin solutions were sucked into borosilicate glass capillary tubes of 1 mm diameter, especially manufactured (Charles Supper, Natick, MA). X-ray scattering experiments require well-aligned samples. The alignment of F-actin filaments could be achieved through the small shear-flow due to sample sucking. The capillaries were then flame-sealed and systematically checked by polarized-light microscopy for alignment and homogeneity before performing x-ray scattering experiments.

Samples in optical and x-ray sealed capillaries were used a few days after preparation to avoid possible actin degradation.

Methods of observation

Optical microscopy

Optical microscopy observations in polarized white light at different magnifications (50×–400×) were performed on a microscope (BX51, Olympus, Tokyo, Japan) equipped with a rotating stage. Liquid-crystalline textures of samples, placed between crossed polarizers, were photographed using a digital camera (Camedia, Olympus) directly mounted on the microscope.

Filaments length measurements

Actin filaments were fluorescently labeled by incubating 1 μM F-actin with one molar equivalent rhodamine-phalloidin (Fluka, St. Louis, MO) for 1 min before dilution to 20 nM in F buffer. Samples were observed in epifluorescence microscopy with a 100× immersion oil objective on a microscope (AX70, Olympus) equipped with a CCD camera (CoolSnapHQ, Roper Scientific, Munich, Germany). Average filaments length was measured using Metamorph software (Universal Imaging, Downingtown, PA) on a population of 100–500 filaments per sample.

Birefringence measurements

We performed a birefringence measurement on a well-aligned sample (prepared for small-angle x-ray scattering experiments) at a very high concentration (310 μM) in a cylindrical capillary, using a microscope equipped with a compensator.

Small-angle x-ray scattering (SAXS)

SAXS measurements were performed on the ID02 beamline of the European Synchrotron Radiation Facility (ESRF), Grenoble, France (30). Oriented domains of millimetrer size were first located with polarized-light microscopy and subsequently placed in the x-ray beam. The incident wavelength was $\lambda = 0.0995$ nm. Due to the high intensity, single 0.1–1 s exposures were found sufficient to record the SAXS signals. The two-dimensional patterns were recorded at a sample/detector distance of 10 m, on a homemade FreLoN CCD camera (ESRF) coupled to a x-ray image intensifier tube (XRII, Thomson, Huizhou, Guangdong province, China) with a resolution of 1024 × 1024 pixels and 165 μm/pixel. Incident and transmitted fluxes were simultaneously recorded with each pattern. Data collection includes recently developed on-line detector and beam-intensity-related corrections already well described (30). One-dimensional azimuthal averaging was used for immediate examination of the data and the SAXS signals were plotted versus scattering-vector modulus $q = (4\pi/\lambda)\sin\Theta$ where 2Θ is the scattering angle. Isointensity contour plots were obtained from the SAXS patterns using the Fit2D package (ESRF).

RESULTS

The birefringence increases gradually with actin concentration

The texture photographs of a capillary series of increasing F-actin concentrations (45–330 μM) are shown in Fig. 1 *A*. When placed between two crossed polarizers, a sample displays birefringence when the molecules form an aligned structure whose main direction is called the nematic director. If there is no preferred orientation, the sample is isotropic and appears dark as the transmitted-light polarization is not changed through the solution. In our case, birefringence was hardly detected at 45 μM F-actin and increased with F-actin concentration in a continuous fashion. A highly birefringent texture was observed at 330 μM F-actin. Coexisting birefringent and isotropic domains were never seen. The same behavior has already been reported on similar suspensions of actin filaments (31–36). The optical textures of concentrated samples are actually very typical of a nematic phase, which previously allowed the identification of this liquid-crystalline type in the absence of any x-ray scattering data.

Although the filaments in these samples are usually slightly aligned along the capillary axis, observations at high magnification reveal the existence of defects called disclination lines of strength (1/2) (Fig. 1 *B*). These topological defects are typically observed in nematic phases of small molecules and polymers as well. They correspond to rotational discontinuities of the nematic director field and

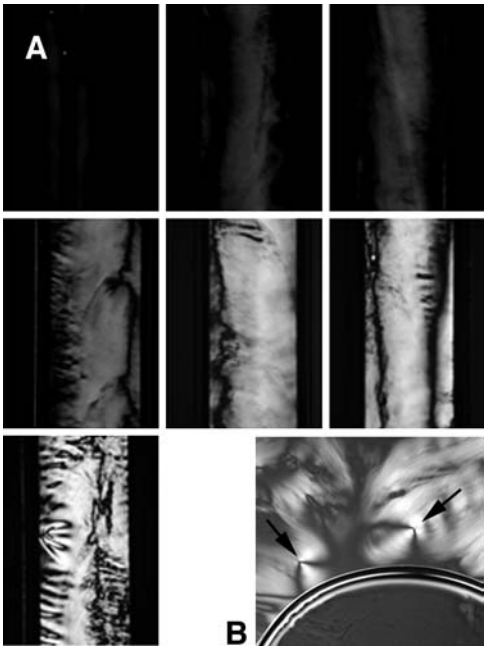

FIGURE 1 (*A*) Birefringent textures of F-actin gels in flat capillaries (100-μm thick and 1-mm wide) observed with polarized light (from *left* to *right* and *top* to *bottom*, increasing actin concentrations are 45, 60, 75, 85, 100, 150, and 330 μM, respectively). (*B*) Detail of the texture of a 50-μM F-actin gel that shows disclination lines (*solid arrows*), typical of nematic liquid crystals. (The *curved line* at the *bottom* is a bubble edge.)

are, in nematic phases, the equivalent of dislocation lines in crystals (20).

The birefringence of actin gels depends on mechanical history

Fig. 2 shows photographs in polarized light of a series of test tubes filled with F-actin gels of increasing concentrations (25–250 μM) before and after various periods of rest and sonication. Right after preparation (Fig. 2 *A*), the birefringence of the samples increases regularly with F-actin concentration, as already observed with samples held in flat capillaries. Many strong distortions of the nematic director are visible because the filaments are not uniformly aligned at the macroscopic scale of the test tubes. Indeed, when rotating the tubes, one observes that the birefringent patterns change, i.e., that ''dark'' regions can appear bright and vice versa. This observation proves that the actin gels are made of many distinct domains with different preferred orientations. A similar methodology was used in a study of the nematic ordering of microtubules suspensions by Hitt et al. (37). In addition to the birefringence photographs, we plotted in Fig. 2 *I* the average transmitted polarized-light intensity (in arbitrary units) as a function of the actin concentration (*solid squares*). For each tube, the intensity was measured both in a region that corresponded to the entire tube (excluding the meniscus and the bottom) or in a smaller square region set at different places in the tube; when normalized to the measured surface area, the average intensity varied by ~15 a.u. (defining the *error bars* in Fig. 2 *I*). (This measurement represents an estimate of the solution birefringence; in the absence of single domains, these birefringence values have only a semiquantitative meaning. However, they illustrate well the visual impression displayed by the test tubes.) The samples did not change over periods of many hours (Fig. 2 *B*), even days (data not shown). Then, all samples were submitted to sonication for a few seconds and immediately examined (Fig. 2 *C* and 2 *I*, *open circles*). The birefringence of the samples at concentrations <100 μM disappeared completely; at concentrations ≥ 100 μM, the birefringence could not be completely erased. In comparison with the state before sonication, the birefringence was clearly weaker for the lowest concentration (100 μM), and was somewhat weaker for the 125 μM sample, but hardly decreased for the three most concentrated tubes (150–250 μM). Nevertheless, the birefringent textures were deeply affected by the sonication (as can be judged by closely comparing Fig. 2, *B* and *C*). The samples were left to rest for 24 h (Fig. 2, *D* and *I*, *open triangles*): the samples that had lost birefringence upon sonication remained isotropic; the birefringence of the 100 μM and, to a lesser extent, 125 μM samples clearly increased during the resting period even though it was not disturbed; no change was visible at higher concentrations (150–250 μM). At this point, all the samples were gently shaken upside-down once (Fig. 2 *E*), which restored birefringence patterns similar to those observed in the earlier stage of the experiment, immediately after sample preparation (Fig. 2 *A*). The texture of all samples remained unaltered for 60 h thereafter (Fig. 2 *F*). The same behavior was recorded upon subsequent repeated cycles of sonication and rest (Fig. 2, *G* and *H*). In conclusion, the birefringence level of all the samples up to 75 μM depends strongly on their mechanical history and can be induced or abolished at will by gentle shaking and sonication, respectively. At 100 μM and 125 μM the birefringence decreases under sonication but increases again under rest. At 150 μM and beyond, although the samples textures are strongly altered by sonication, the birefringence level is not affected.

A detailed interpretation of these data is provided in Discussion, below.

SAXS patterns of F-actin gels show clear anisotropy but no interference peak

Well-aligned samples of F-actin gels were obtained by sucking material into cylindrical x-ray capillaries. When observed between crossed polarizers, these samples look dark when their main axis is parallel to either one of the polarizer directions and look uniformly bright when their axis lies at a 45° angle from these directions (Fig. 3). This behavior characterizes well-aligned nematic samples (20). The best aligned samples were obtained at the highest F-actin

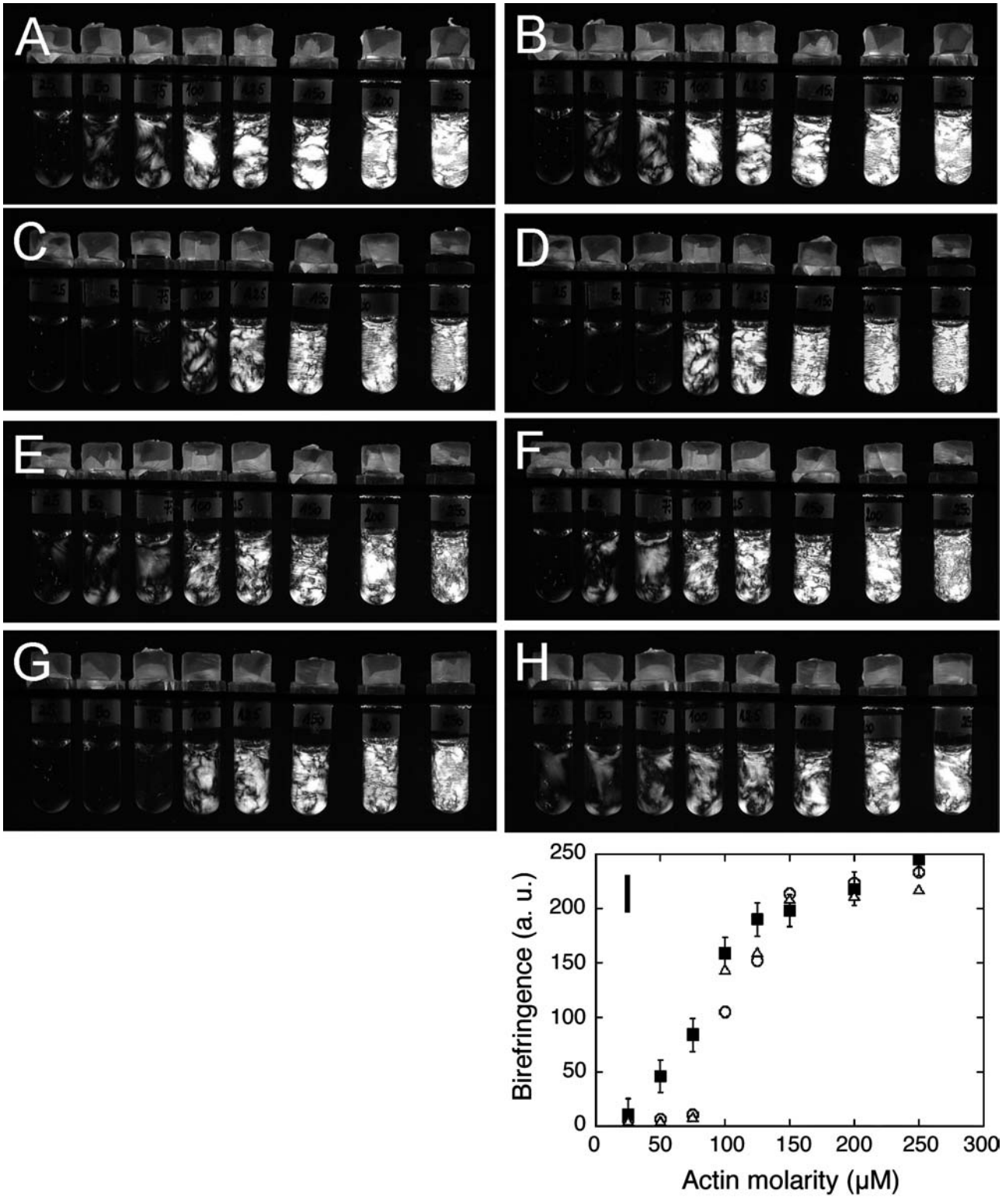

FIGURE 2 (*A–H*) Birefringence of F-actin gels in test tubes (25, 50, 75, 100, 125, 150, 200, and 250 μM, from *left* to *right*, respectively): (*A*) right after polymerization, (*B*) after 24 h, (*C*) after 10 s sonication, (*D*) 24 h after sonication, (*E*) slightly shaken, (*F*) after 60 h, (*G*) 24 h after a second 10-s sonication, and (*H*) slightly shaken. (*I*) Average transmitted polarized light, in arbitrary units, as a function of actin concentration in *A*, solid squares; *C*, open circles; and *D*, open triangles. Note the intensity increase between *C* and *D* for the 100- and 125-μM tubes. The error bars (shown only for the *solid squares* for clarity) were estimated by comparing the intensity transmitted through the entire tube and through smaller square regions set at different places of the tube. As explained in the text, the samples are not single domains and this measurement only represents an estimate of the solutions birefringence.

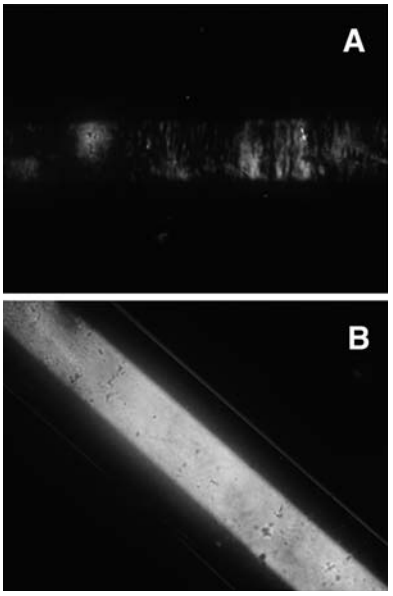

FIGURE 3 The 150-μM actin gel aligned in a cylindrical x-ray capillary observed with polarized light: the main axis is (*A*) parallel to the direction of one of the crossed polarizers, and (*B*) oriented at 45° with respect to the polarizer directions.

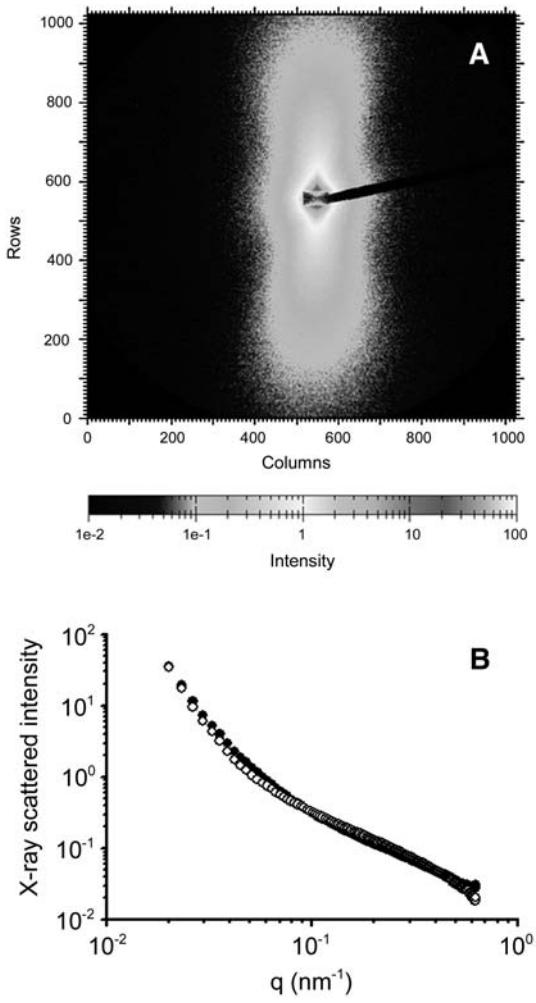

FIGURE 4 (*A*) X-ray pattern measured for an actin concentration of 310 μM. The pattern anisotropy is clearly visible. The bottom grayscale indicates the scattered intensity increasing from left to right. (*B*) X-ray scattered intensity I in absolute units (mm^{-1}) versus scattering vector modulus q in log-log scale, for actin solutions of 310 μM (*solid circles*) and 150 μM (*open circles*). For comparison purposes the curves were superposed by dividing the data by the respective actin concentrations. Note the absence of a peak that would characterize any positional order in the solution.

concentration (310 μM), but sucking the actin gels in capillaries produced fair alignments of filaments at actin concentrations as low as 25 μM.

All samples run at the ID02 experimental station of ESRF displayed rather weak but very anisotropic SAXS patterns (Fig. 4 *A*). Radiation damage was found negligible except for the two least concentrated samples that nevertheless displayed consistent patterns. By radially averaging the scattering pattern, the intensity profile $I(q)$ could be plotted and we show on Fig. 4 *B* absolute measurements of the SAXS signals, at two actin molarities: 150 μM and 312 μM. No x-ray scattering peak that would correspond to any, even short-range, positional order of the filaments, was recorded at any concentration. Instead, the scattered intensity regularly decreased with increasing scattering vector modulus. One can characterize the orientational order of the actin gels by extracting the isointensity contour lines from the x-ray patterns (Fig. 5). The contour lines' anisotropy is analyzed in Discussion, below.

DISCUSSION

Let us first discuss the series of experiments with test tubes, illustrated in Fig. 2. We distinguish two different behaviors and consider therefore two groups of test tubes. First, we examine the three least concentrated solutions (25–75 μM).

Birefringence is related to the gel properties of actin

Our observations show that up to 75 μM F-actin, birefringence of actin gels results from shear-induced alignment of filaments. In other words, birefringence depends on the mechanical history of the sample and does not have a thermodynamic basis, at variance with a previous statement (23). The birefringence of actin gels is strongly dependent on the handling of the samples, which explains discrepancies in the literature. Samples devoid of residual stresses are very hard to obtain. Indeed, some studies of F-actin gels rely on experimental procedures that involve strong sample flows meant to increase the birefringence through filament alignment. The resulting birefringent patterns are frozen over periods of several months because the elasticity of the gel prevents relaxation to the isotropic state. A somewhat similar situation prevails for aqueous clay gels that are birefringent but do not show a true isotropic/nematic phase coexistence (38–40).

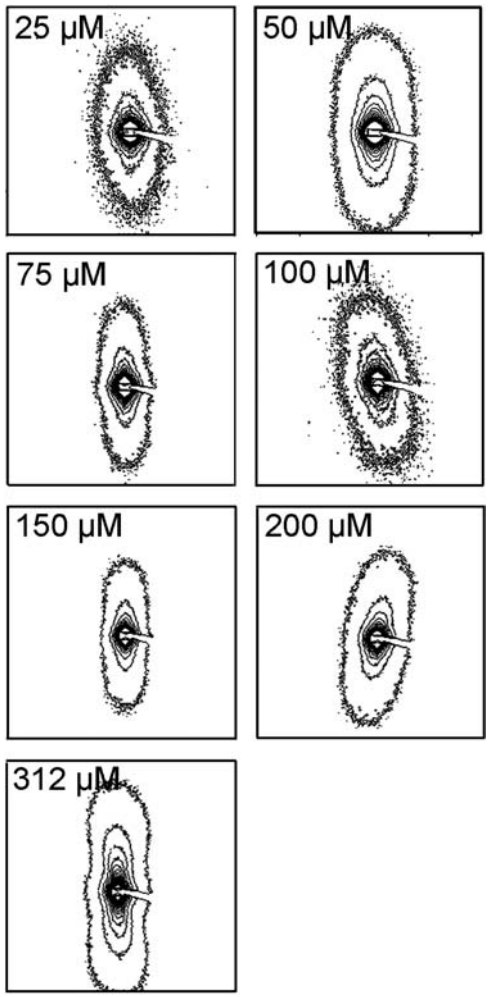

FIGURE 5 Isointensity contours of the x-ray patterns measured upon increasing actin concentrations from 25 μM to 310 μM. These patterns are all anisotropic, even at the lowest concentration, which indicates strong filament orientation. (An isointensity contour is a line along which the pattern has the same intensity.)

Mechanical history can be erased by sonication

Actin filaments are severed into short fragments by sonication. Under continuous sonication at a given power, filaments are maintained at a constant average length that results from a balance between fragmentation (a first-order reaction, with rate constant k_f) and end-to-end reannealing (a second-order reaction, with rate constant k_r), as described by the equation

$$F_i + F_j \underset{k_f}{\overset{k_r}{\rightleftarrows}} F_{i+j}.$$

The average length under sonication is expected to increase with F-actin concentration, due to the increasing rate of end-to-end reannealing. When sonication is arrested, both end-to-end reannealing and length redistribution via monomer-polymer exchange take place, leading to the reestablishment of a population of longer filaments (41). Measurements of filament length under and right after sonication had so far been performed in a concentration range of 0–10 μM F-actin (41). Here we verified that the average length under sonication increases with actin concentration (Fig. 6), suggesting that rapid end-to-end reannealing of filaments takes place under sonication at all actin concentrations. However, it reached a constant value of $\sim$7 μm above 100 μM F-actin. When sonication was stopped, the average length after 24 h's rest did not increase beyond the value of $\sim$8 μm, even at very high actin concentrations (Fig. 6). These limited average lengths, under and after sonication, suggest that the viscosity of the actin gels at high concentration strongly slows down the reannealing reaction. Sonication has been used here as a unique opportunity to erase the samples mechanical history. The recovery of the sample birefringence upon gentle shaking demonstrates that the F-actin filaments have indeed reannealed. ATP is gradually exhausted during the cycles of sonication-resting. However, the critical concentrations for assembly of ATP-actin (0.1 μM) and ADP-actin (1.5 μM) are both much lower than the total actin concentration in all samples. Thus we may consider that the concentration of F-actin is constant in all experiments.

Spontaneous nematic ordering occurs at high actin concentrations

We now turn to the five most concentrated samples (100–250 μM) the birefringence of which could never be completely erased by sonication (Fig. 2, *C*, *G*, and *I*). This is most probably due to the fast end-to-end reannealing of the severed filaments under continuous sonication at high concentration, as explained above. However, the 100- and 125-μM samples behaved differently from the 150–250 μM ones. At the former concentrations, the birefringence clearly decreased under sonication (Fig. 2, *C* and *I*). Moreover, most

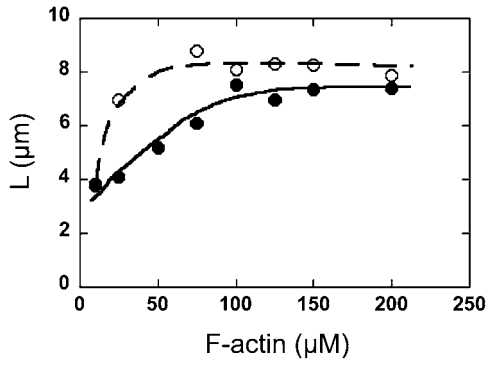

FIGURE 6 Average filaments length under continuous sonication (*solid circles*) and 24 h after sonication (*open circles*) at varying concentrations of F-actin (10–200 μM). For the measurement under sonication, F-actin is pipetted in the test tube after 30-s sonication, while the probe is still sonicating, and directly diluted to 1 μM in F-buffer in presence of 1 μM rhodamine-phalloidin.

importantly, the birefringence spontaneously increased on a timescale of hours, even though the samples were left completely undisturbed (Fig. 2, *D* and *I*). This phenomenon is less obvious for the 125 μM sample in Fig. 2 *I* that shows semiquantitative birefringence intensity measurements. At concentrations $\geq$150 μM, strong flows and textures changes were clearly visible during sonication, proving that the actin gels were effectively disrupted. Nevertheless, the birefringence intensity, averaged over sample texture, was not altered after sonication. The spontaneous birefringence recovery of the 100- and 125-μM samples is a clear sign that, at high enough F-actin concentration, the alignment of actin filaments is of thermodynamic origin. However, the isotropic/nematic macroscopic phase separation does not occur because it would require the large-scale diffusion of filaments and their gathering in domains. This process is severely hampered by the viscoelasticity of these gels.

These observations imply that, at variance with a previous report (23), the intrinsic nematic ordering of actin filaments does not occur at a molarity of 25 or 50 μM, but rather between 75 and 150 μM, in better agreement with the Onsager model predictions of the *I-N* transition (42,21). Indeed, according to Onsager's theory, the volume fractions of the isotropic and nematic phases, ϕ_i and ϕ_n, at the transition are given by $\phi_i = 3.3D/L$ and $\phi_n = 4.2D/L$, where D and L are the filament diameter and length, respectively. Onsager's model that is valid for stiff rods was extended by Khokhlov and Semenov (43) for the case of semiflexible polymers like actin. Their results are fairly similar to those of Onsager, but the volume fractions at coexistence are expressed by $\phi_i = 5.1D/L_p$ and $\phi_n = 5.5D/L_p$, where L_p is the polymer persistence length. Using the values $D = 8$ nm and $L_p = 10$ μm, the theoretical values $\phi_i = 4.1 \times 10^{-3}$ and $\phi_n = 4.4 \times 10^{-3}$ are predicted in very good agreement with the experimental range of 75–150 μM that corresponds to a ϕ-range of 3–6 $\times$ 10^{-3}. Note that the influence of electrostatic interactions is negligible at the high ionic strengths of these suspensions ($I > 0.1$ M) that were fixed close to physiological conditions.

Actin gels show no positional order

Let us now turn to the SAXS patterns of aligned actin gels shown in Figs. 4 and 5. Since all scattering measurements were calibrated on an absolute scale, the effect of concentration can be directly assessed. Once divided by the concentration, the intensity curves superimpose fairly well for the four most concentrated (100–310 μM) samples. (The intensity increase close to the beam-stop is due to some parasitic scattering. The SAXS signals of the three least concentrated samples, i.e., 25–75 μM, are weaker and would require a more elaborate background subtraction to obtain curves comparable to those at high concentrations; data not shown.) As already briefly mentioned in Results, above, the absence of any peak in $I(q)$ and the fact that the normalized SAXS signals do not depend on concentration (Fig. 4 *B*) demonstrate the absence of any interferences between different filaments. Thus, there is no liquidlike positional order characterized by a typical distance between the filaments. This may be due to two reasons: The high ionic strength ($I > 10^{-1}$ M) of the suspensions, close to physiological conditions, effectively screens the electrostatic repulsions between colloidal charged objects, which is known to suppress the short-range liquidlike order. Besides, gelation may freeze the positional fluctuations and therefore may prevent the establishment of the positional liquidlike order, as observed in clay gels. Due to the absence of positional correlations between actin filaments, the scattered intensity is governed by the filament form factor and the structure factor is flat (44).

The nematic order is strong

As there is no sign of interparticle positional correlation, we can discuss the x-ray patterns in terms of the convolution of the form factor of actin filaments by a nematic orientational distribution function. A similar approach was successfully applied to shear-aligned surfactant micelles and clay gels (45,46). This method allows one to extract the nematic order parameter S from the scattering patterns. (The nematic order parameter S is the second moment of the orientational distribution function; it takes values ranging from 0 for an isotropic phase to 1 for a perfectly aligned nematic phase; see De Gennes and Prost (20).)

Actin filaments are crudely modeled as uniform cylinders of length L and diameter $D = 2R$. Their form factor is then classically given by the expression (44)

$$F(q,\gamma) = K\frac{\sin(qL\cos\gamma)}{qL\cos\gamma}\frac{J_1(qR\sin\gamma)}{qR\sin\gamma},$$

where K is a constant that includes the electron density contrast between the particles and the solvent, J_1 is the first-order Bessel function, and γ is the angle between the cylinder axis **n** and the scattering vector **q** (Fig. 7).

We call θ and φ the polar and azimuthal angles of the cylinder axis **n** in a system of coordinates where the z axis is taken along the nematic director and the y axis along the incident x-ray beam. We call ψ the angle between **q** and the x axis (Fig. 7). These angles are then related by

$$\cos\gamma = \cos\theta\sin\psi + \sin\theta\cos\psi\cos\varphi.$$

We adopt the classical Maier-Saupe form for the orientational distribution function (47–49),

$$f(\theta) = \frac{1}{Z}\exp(m\cos^2\theta),$$

where Z is a normalization constant and m is the Maier-Saupe distribution parameter that is directly related to S.

We then average the form factor using this distribution function, which directly gives us the expression of the scattered intensity

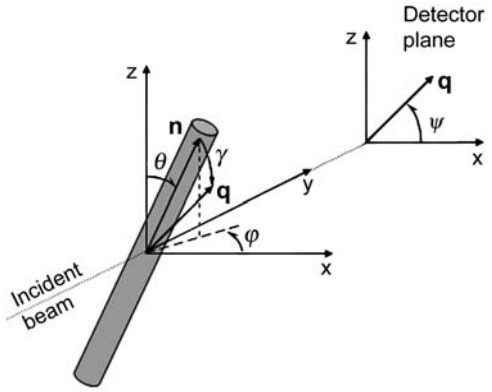

FIGURE 7 Schematic representation of the scattering experiment that shows the definitions of the angular coordinates referred to in the text. The shaded cylinder represents an actin filament.

$$I(\mathbf{q}) = I(q,\psi) = 2K^2 \int_0^{2\pi} d\varphi \int_0^{\frac{\pi}{2}} f(\theta)F^2(q,\gamma)\sin\theta\, d\theta.$$

The experimental SAXS isointensity lines (Fig. 5) can be compared with those calculated with this model, using the MATHEMATICA 4.0 software (Wolfram Research, Champaign, IL), to extract the values of m and S (Fig. 8). We used the value $D = 8$ nm that is commonly accepted for the actin filament diameter. To minimize calculation times, we chose $L = 500$ nm for the filament length, a value that is much lower than usually reported in such conditions ($\sim$1–10 μm). Fortunately, the calculated pattern is very little sensitive to L in this range and this should not significantly alter the values of S that we obtained. In contrast, the pattern anisotropy is very sensitive to the value of S, which allows us to deduce it fairly accurately. Note that the simulations reveal a small dip of the isointensity lines on the horizontal axis, which is not observed on the experimental patterns, except on some of the isointensity lines of the 310-μM sample (Fig. 5). Such a dip has been observed and modeled by Cummins et al. (50) in their neutron scattering study of rodlike surfactant micelles aligned by shear flow. In our case, the dip is usually not observed probably due to some parasitic scattering, close to the beam-stop, that hides the weak signal of F-actin suspensions.

In the case of the 310-μM sample (Fig. 5, *bottom left*), we derive a large nematic order parameter $S = 0.70 \pm 0.05$, which agrees well with the large anisotropy of the pattern. Such a value of $S = 0.7$ means that 70% of the actin filaments make an angle $<30°$ with their average direction (director). This value of S should be compared with those of other lyotropic nematic phases of semiflexible polymers such as the suspensions of fd viruses ($0.60 \leq S \leq 0.95$) (51), or with that of nematic solutions of microtubules (0.81) (37), and with the theoretical value of 0.80 predicted by the Onsager model (42). We thus find an order parameter of the correct magnitude even though the sample is not truly a single domain. The nematic order parameters derived from the other SAXS patterns are lower and range from 0.4 to 0.5, depending not only on molarity but also, most probably, on the quality of sample alignment. Nevertheless, the value $S = 0.40 \pm 0.05$, obtained for the fairly dilute 25-μM sample, is still quite appreciable and is in fact comparable to the S-values of common liquid crystals used in display applications (20). These strong values of the order parameter indicate that either a small shear flow (for low concentrations) or even spontaneous nematic alignment (for high concentrations) can produce highly oriented filament assemblies in the absence of ABPs. Moreover, this filament alignment most probably helps the bundling action of some ABPs such as α-actinin.

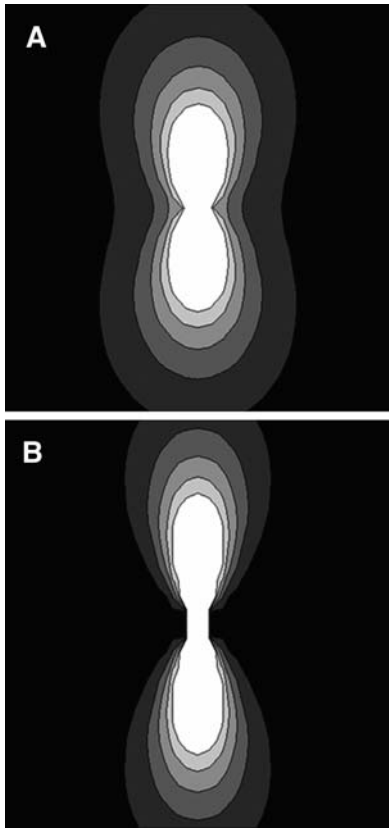

FIGURE 8 Calculated isointensity lines using $D = 8$ nm and $L = 500$ nm as cylinder parameters. The nematic order parameter for these computations is (*A*) $S = 0.45$; (*B*) $S = 0.7$.

As a last result, we also measured the specific birefringence of actin filaments from the most concentrated sample (310 μM) whose SAXS pattern is shown in Fig. 5, because it was the best aligned and most birefringent sample. For a dilute ($\phi < 1\%$) suspension of particles smaller than the wavelengths of visible light, the birefringence Δn is related to the nematic order parameter by $\Delta n = \Delta n_{\text{sat}}\, \phi\, S$, where Δn_{sat} is the specific birefringence of the particles. A birefringence Δn of 2.1×10^{-4} was measured for the 310-μM sample. This allowed us to derive the specific birefringence of actin filaments, $\Delta n_{\text{sat}} = 2.25 \times 10^{-2}$, a value

quite comparable to that (1.7×10^{-2}) of the tobacco mosaic virus (52).

CONCLUSION

We performed SAXS experiments that demonstrate that the nematic order parameter takes large values (0.4–0.7) in the whole investigated range of molarities (25–300 μM) instead of the very low values predicted for a continuous *I-N* transition (24). Using polarized-light techniques, we also showed that the gradual onset of birefringence in actin gels of molarities <100 μM is not of thermodynamic origin but is rather due to residual mechanical stresses. However, these materials certainly undergo some kind of nematic ordering at molarities ≥ 100 μM but their strong viscoelastic properties restrict the phase transition to a microscopic scale, as already suggested by another group (22). Both results, from SAXS and birefringence experiments, lead us to conclude that actin gels are not a good example of a continuous isotropic-to-nematic phase transition. Nevertheless, our work demonstrates that, for molarities of 100 μM or more, spontaneous parallel organization of actin filaments occurs.

The spontaneous appearance of large aligned domains in concentrated actin gels may play a role in the rapid formation of parallel structures like tight bundles in stress fibers or microvilli, because the diffusion of linear objects is known to be much faster when they are cooperatively oriented, a well-known specific feature of nematic liquid crystals. Similarly, the growth of filaments may be expected to be faster if they are aligned rather than entangled. Spontaneous nematic alignment, shear flow effects, and ABPs are all factors that can take part in the formation of oriented actin structures. The study reported here was required for us to understand the nematic behavior of pure actin at physiological concentrations and will help us to assess the respective influences of each of these factors. In vivo, the actin arrays linked to diverse motile or adhesive processes are organized at a higher level of complexity by a variety of regulatory proteins, like Actin Depolymerizing Factor (ADF/cofilin), which accelerates the treadmilling of actin filaments and may affect their mechanical properties; Arp2/3 complex, which is involved in branching filaments thus affecting the intrication of actin gels; and capping proteins, which regulate filament length. Further experimentation will be carried out to obtain insight into the effect of these regulators on the behavior of actin gels. For example, two machineries are known to initiate actin filaments at the cell membrane, namely the above-mentioned Arp2/3 complex and the more recently discovered group of formins: the first one generates the growth of a branched actin array (53), whereas the second one was shown to promote the nucleation of unbranched actin filaments (54). Depending on whether the actin concentration is well below or well above 100 μM, we expect some influence of the filament alignment on the nucleating activities of these two systems.

We are grateful to P. Bösecke, A. Hammersley, and R. Wilcke for on-line data corrections and treatment software packages, and N. Dupuis for help with the simulation computer programs. We thank I. Dozov for the birefringence measurement.

REFERENCES

1. Pollard, T. D., L. Blanchoin, and R. D. Mullins. 2000. Molecular mechanisms controlling actin filament dynamics in nonmuscle cells. *Annu. Rev. Biophys. Biomol. Struct.* 29:545–576.
2. Oosawa, F., and S. Asakura. 1975. Thermodynamics of the Polymerization of Protein. Academic Press, New York.
3. Korn, E. D., M.-F. Carlier, and D. Pantaloni. 1987. Actin polymerization and ATP hydrolysis. *Science.* 238:638–644.
4. Limozin, L., and E. Sackmann. 2002. Polymorphism of cross-linked actin networks in giant vesicles. *Phys. Rev. Lett.* 89:168103-1–168103-4.
5. Pelletier, O., E. Pokidysheva, L. S. Hirst, N. Bouxsein, Y. Li, and C. R. Safinya. 2003. Structure of actin cross-linked with α-actinin: a network of bundles. *Phys. Rev. Lett.* 91:148102-1–148102-4.
6. Renault, A., P. F. Lenne, C. Zakri, A. Aradian, C. Venien-Bryan, and F. Amblard. 1999. Surface-induced polymerization of actin. *Biophys. J.* 76:1580–1590.
7. Helfer, E., S. Harlepp, L. Bourdieu, J. Robert, F. C. MacKintosh, and D. Chatenay. 2000. Microrheology of biopolymer-membrane complexes. *Phys. Rev. Lett.* 85:457–460.
8. Wong, G. C. L., J. X. Tang, A. Lin, Y. Li, P. A. Janmey, and C. R. Safinya. 2000. Hierarchical self-assembly of F-actin and cationic lipid complexes: stacked three-layer tubule networks. *Science.* 288:2035–2039.
9. Limozin, L., M. Bärmann, and E. Sackmann. 2003. On the organization of self-assembled actin networks in giant vesicles. *Eur. Phys. J. E.* 10:319–330.
10. Farge, E., and A. C. Maggs. 1993. Dynamics scattering from semiflexible polymers. *Macromolecules.* 26:5041–5044.
11. Ott, A., M. Magnasco, A. Simon, and A. Libchaber. 1993. Measurement of the persistence length of polymerized actin using fluorescence microscopy. *Phys. Rev. E.* 48:R1642–R1645.
12. Isambert, H., P. Venier, A. C. Maggs, A. Fattoum, R. Kassab, D. Pantaloni, and M.-F. Carlier. 1995. Flexibility of actin filaments derived from thermal fluctuations. Effect of bound nucleotide, phalloidin, and muscle regulatory proteins. *J. Biol. Chem.* 270: 11437–11444.
13. MacKintosh, F., J. Käs, and P. A. Janmey. 1995. Elasticity of semiflexible biopolymer networks. *Phys. Rev. Lett.* 75:4425–4428.
14. Isambert, H., and A. C. Maggs. 1996. Dynamics and rheology of actin solutions. *Macromolecules.* 29:1036–1040.
15. Morse, D. C. 1998. Viscoelasticity of tightly entangled solutions of semiflexible polymers. *Phys. Rev. E.* 58:R1237–R1240.
16. Amblard, F., A. C. Maggs, B. Yurke, A. N. Pargellis, and S. Leibler. 1996. Subdiffusion and anomalous local viscoelasticity in actin networks. *Phys. Rev. Lett.* 77:4470–4473.
17. Schnurr, B., F. Gittes, F. C. MacKintosh, and C. F. Schmidt. 1997. Determining microscopic viscoelasticity in flexible and semiflexible polymer networks from thermal fluctuations. *Macromolecules.* 30: 7781–7792.
18. Gisler, T., and D. A. Weitz. 1999. Scaling of the microrheology of semidilute F-actin solutions. *Phys. Rev. Lett.* 82:1606–1609.
19. Helfer, E., S. Harlepp, L. Bourdieu, J. Robert, F. C. MacKintosh, and D. Chatenay. 2001. Viscoelastic properties of actin-coated membranes. *Phys. Rev. E.* 63:021904-1–021904-13.
20. De Gennes, P.-G., and J. Prost. 1994. The Physics of Liquid Crystals. Clarendon, Oxford, UK.

21. Vroege, G. J., and H. N. W. Lekkerkerker. 1992. Phase transitions in lyotropic colloidal and polymer liquid crystals. *Rep. Prog. Phys.* 55: 1241–1309.

22. Käs, J., H. Strey, J. X. Tang, D. Finger, R. Ezzell, E. Sackmann, and P. A. Janmey. 1996. F-actin, a model polymer for semiflexible chains in dilute, semidilute, and liquid crystalline solutions. *Biophys. J.* 70: 609–625.

23. Viamontes, J., and J. X. Tang. 2003. Continuous isotropic-nematic liquid crystalline transition of F-actin solutions. *Phys. Rev. E.* 67: R040701-1–R040701-4.

24. Lammert, P. E., D. S. Rokhsar, and J. Toner. 1993. Topology and nematic ordering. *Phys. Rev. Lett.* 70:1650–1653.

25. Lammert, P. E., D. S. Rokhsar, and J. Toner. 1995. Topology and nematic ordering. I. A gauge theory. *Phys. Rev. E.* 52:1778–1800.

26. Toner, J., P. E. Lammert, and D. S. Rokhsar. 1995. Topology and nematic ordering. II. Observable critical behavior. *Phys. Rev. E.* 52: 1801–1810.

27. Abraham, V. C., V. Krishnamurthi, D. Lansing Taylor, and F. Lanni. 1999. The actin-based nanomachine at the leading edge of migrating cells. *Biophys. J.* 77:1721–1732.

28. Wiesner, S., E. Helfer, D. Didry, G. Ducouret, F. Lafuma, M.-F. Carlier, and D. Pantaloni. 2003. A biomimetic motility assay provides insight into the mechanism of actin-based motility. *J. Cell Biol.* 160: 387–398.

29. Spudich, J. A., and S. Watt. 1971. The regulation of rabbit skeletal muscle contraction. I. Biochemical studies of the interaction of the tropomyosin-troponin complex with actin and the proteolytic fragments of myosin. *J. Biol. Chem.* 246:4866–4871.

30. Narayanan, T., O. Diat, and P. Bösecke. 2001. SAXS and USAXS on the high brilliance beamline at the ESRF. *Nucl. Instr. Meth. Phys. Res. A.* 467–468:1005–1009.

31. Buxbaum, R. E., T. Dennerll, S. Weiss, and S. R. Heidemann. 1987. F-Actin and microtubule suspensions as indeterminate fluids. *Science.* 23:1511–1514.

32. Kerst, A., C. Chmielewski, C. Livesay, and R. E. Buxbaum. 1990. Liquid crystal domains and thixotropy of filamentous actin suspensions. *Proc. Natl. Acad. Sci. USA.* 87:4241–4245.

33. Suzuki, A., T. Maeda, and T. Ito. 1991. Formation of liquid crystalline phase of actin filament solutions and its dependence on filament length as studied by optical birefringence. *Biophys. J.* 59:25–30.

34. Coppin, C. M., and C. P. Leavis. 1992. Quantitation of liquid-crystalline ordering in F-actin solutions. *Biophys. J.* 63:794–807.

35. Furukawa, R., R. Kundra, and M. Fechheimer. 1993. Formation of liquid crystals from actin filaments. *Biochemistry.* 32:12346–12352.

36. Oda, T., K. Makino, I. Yamaschita, K. Namba, and Y. Maéda. 1998. Effect of the length and effective diameter of F-actin on the filament orientation in liquid-crystalline sols measured by x-ray fiber diffraction. *Biophys. J.* 75:2672–2681.

37. Hitt, A. L., A. R. Cross, and R. C. Williams, Jr. 1990. Microtubule solutions display nematic liquid crystalline structure. *J. Biol. Chem.* 265:1639–1647.

38. Langmuir, I. 1938. The role of attractive and repulsive forces in the formation of tactoids, thixotropic gels, protein crystals and coacervates. *J. Chem. Phys.* 6:873–896.

39. Mourchid, A., A. Delville, J. Lambard, E. Lécolier, and P. Levitz. 1995. Phase diagram of colloidal dispersions of anisotropic charged particles: equilibrium properties, structure, and rheology of laponite suspensions. *Langmuir.* 11:1942–1950.

40. Gabriel, J. C. P., C. Sanchez, and P. Davidson. 1996. Observation of nematic liquid-crystal textures in aqueous gels of smectite clays. *J. Phys. Chem.* 100:11139–11143.

41. Carlier, M.-F., D. Pantaloni, and E. D. Korn. 1985. Polymerization of ADP-actin and ATP-actin under sonication and characteristics of the ATP-actin equilibrium polymer. *J. Biol. Chem.* 260:6565–6571.

42. Onsager, L. 1949. The effects of shape on the interaction of colloidal particles. *Ann. N. Y. Acad. Sci.* 51:627–659.

43. Khokhlov, A. R., and A. N. Semenov. 1981. Liquid-crystalline ordering in the solution of long persistent chains. *Physics.* 108A:546–556.

44. Guinier, A. 1994. X-Ray Diffraction in Crystals, Imperfect Crystals and Amorphous Bodies. Dover, Mineola, NY.

45. Hayter, J. B., and J. Penfold. 1984. Use of viscous shear alignment to study anisotropic micellar structure by small angle neutron scattering. *J. Phys. Chem.* 88:4589–4593.

46. Lemaire, B. J., P. Panine, J. C. P. Gabriel, and P. Davidson. 2002. The measurement by SAXS of the nematic order parameter of laponite gels. *Europhys. Lett.* 59:55–61.

47. Maier, W., and A. Saupe. 1958. A simple molecular-statistics theory of the nematic liquid-crystalline state. *Z. Naturforsch.* 13a:564–566.

48. Maier, W., and A. Saupe. 1959. A simple molecular-statistics theory of the nematic liquid-crystalline phase. Part I. *Z. Naturforsch.* 14a:882–889.

49. Maier, W., and A. Saupe. 1960. A simple molecular-statistics theory of the nematic liquid-crystalline phase. Part II. *Z. Naturforsch.* 15a:287–292.

50. Cummins, P. G., E. Staples, J. B. Hayter, and J. Penfold. 1987. A small-angle neutron scattering investigation of rod-like micelles aligned by shear-flow. *J. Chem. Soc., Faraday Trans. 1.* 83:2773–2786.

51. Purdy, K., Z. Dogic, S. Fraden, A. Rühm, L. Lurio, and S. G. J. Mochrie. 2003. Measuring the nematic order of suspensions of colloidal fd virus by x-ray diffraction and optical birefringence. *Phys. Rev. E.* 67:031708-1–031708-12.

52. Fraden, S., G. Maret, and D. L. D. Caspar. 1993. Angular correlations and the isotropic-nematic phase transition in suspensions of Tobacco Mosaic Virus. *Phys. Rev. E.* 48:2816–2837.

53. Svitkina, T. M., and G. G. Borisy. 1999. Arp2/3 complex and actin depolymerizing factor/cofilin in dendritic organization and treadmilling of actin filament array in lamellipodia. *J. Cell Biol.* 145:1009–1026.

54. Sagot, I., A. A. Rodal, J. Moseley, B. L. Goode, and D. Pellman. 2002. An actin nucleation mechanism mediated by Bni1 and profilin. *Nat. Cell Biol.* 4:626–631.